Hindawi Publishing Corporation
Journal of Nanomaterials
Volume 2008, Article ID 168716, 9 pages
doi:10.1155/2008/168716

Research Article

The Effect of Stirring on the Morphology of Birnessite Nanoparticles

Marcos A. Cheney,[1,2] Pradip K. Bhowmik,[2] Shingo Moriuchi,[1] Mario Villalobos,[3] Shizhi Qian,[4] and Sang W. Joo[5]

[1] *Department of Health Physics, University of Nevada, Las Vegas, NV 89154, USA*
[2] *Department of Chemistry, University of Nevada, Las Vegas, NV 89154, USA*
[3] *Grupo de Bio-Geoquimica Ambiental, LAFQA, Instituto de Geografia, Ciudad Universitaria, UNAM, Coyoacan 04510, Mexico*
[4] *Department of Aerospace Engineering, Old Dominion University, Norfolk, VA 23529-0247, USA*
[5] *School of Mechanical Engineering, Yeungnam University, Gyeongsan 712-749, South Korea*

Correspondence should be addressed to Sang W. Joo, swjoo@yu.ac.kr

Received 13 February 2008; Accepted 6 May 2008

Recommended by Sang-Hee Cho

The effect of mechanical stirring on the morphology of hexagonal layer-structure birnessite nanoparticles produced from decomposition of $KMnO_4$ in dilute aqueous H_2SO_4 is investigated, with characterization by X-ray diffraction (XRD), scanning electron microscopy (SEM), transmission electron microscopy (TEM), high-resolution transmission electron microscopy (HRTEM), thermogravimetric analysis (TGA), and N_2 adsorption (BET). Mechanical stirring during an initial stage of synthesis is shown to produce black birnessite containing nanofibers, whereas granular particulates of brown birnessite are produced without stirring. This is the first reduction synthesis of black birnessite nanoparticles with dendritic morphology without any use of organic reductant, and suggests that a particular morphology can arise from structural preferences of Mn in acidic conditions rather than particular organic reactants. These results enlighten the possibility of synthesizing nanoparticles with controlled size and morphology.

Copyright © 2008 Marcos A. Cheney et al. This is an open access article distributed under the Creative Commons Attribution License, which permits unrestricted use, distribution, and reproduction in any medium, provided the original work is properly cited.

1. INTRODUCTION

There are increasing interests in layer-structure materials due to their potential applications in catalysis, ion-sieves, and rechargeable batteries [1–3]. Birnessite, a ubiquitous material present in diverse geological settings including ocean nodules, ore deposits, and alteration crusts [4, 5], is a layer-structure manganese oxide with edge-sharing MnO_6 octahedra, and has been a subject of intensive investigations due to its unique cation exchange capacity [6], sorption [7], and redox properties [5, 8]. Synthetic production of birnessite and birnessite-like materials thus has attracted great attentions, with recent focus on the structural or morphology control [5, 9, 10].

A number of different synthetic processes can be used to prepare layer-structure brown birnessite of micron size, including oxidation of Mn(II) in basic solution [11] using O_2, $K_2S_2O_8$, or H_2O_2, redox reaction between Mn(II) and MnO_4^- [12], reduction of MnO_4^- by different routes such as sol gel [13], reaction of HCl with MnO_4^- followed by cationic exchange. All of these methods require addition of one reactant or another [14]. The structure characteristics of birnessite produced, such grain size and morphology, vary with synthetic methods and in many cases with batch to batch even with identical methods of preparation. Like most other syntheses of micro and nanoparticles, the selection mechanism or conditions leading to a particular choice of structure is not yet clearly understood.

The present study reports synthesis of birnessite nanoparticles with hexagonal layer structure, based on the reduction of $KMnO_4$ in aqueous H_2SO_4, followed by wet-aging time and air drying. Although this reaction has been studied intensively [15–18], the detailed synthetic conditions correlated with the structural parameters of birnessite

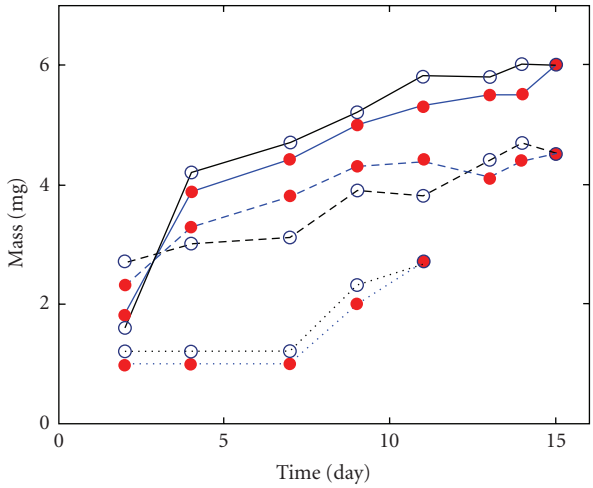

Figure 1: Mass of MnO_2 produced by decomposition of 0.25 M $KMnO_4$ in 0.1 M (solid lines), 0.05 M (dashed lines), and 0.01 M (dotted lines) H_2SO_4 aqueous solution. The solid and open circles represent, respectively, the results in the presence and absence of stirring.

produced have not been reported. To date synthesis of black birnessite nanoparticles, or nanofibers, with dendritic morphology by our direct method (reduction of $KMnO_4$ by H_2SO_4) has not been reported, and it is speculated that dendritic structures produced by other methods are caused by either organic [19] or inorganic [20] reactants. Here, we show that our method produces black birnessite nanoparticles with dendritic morphology as well as the usual brown birnessite. The black birnessite nanoparticles are produced by stirring the solution during an initial stage of the synthesis. The brown birnessite produced as observed by HRTEM correlates well with an existing idealized structural hexagonal model for birnessite constructed from extended X-ray absorption fine structure (EXAFS) spectra. The size and morphology of birnessite particles yielded, or the selection of a preferred state of micro and nanostructure, thus are shown to depend in part on the mechanical conditions of the reacting solution.

In the following sections, we present the synthesis process of black and brown birnessite particles, and show their morphological details using various state-of-the-art characterization techniques available. Discussions on the significance of the results and concluding remarks follow.

2. EXPERIMENT

2.1. Synthesis

The preparation of birnessite is performed by reduction of $KMnO_4$ in the presence of H_2SO_4 in a closed reaction vessel in the absence of light. The experimental procedure is a modification of the method used by Clark and Coe [14] for preparation of MnO_2. All chemicals are analytical grade, and handled with extreme care to avoid any impurities. All pieces of glassware are acid cleaned, and ultrapure water devoid of any organic compounds is used, which is often a critical issue in this type of reaction. Our synthetic procedure involves preparation of acidified $KMnO_4$ solutions in two different initial processes for solution homogenization, mechanical stirring followed by shaking only. Both are then ensued by stationary aging in the dark.

The first set of solutions are prepared by adding 100 mL of 18 MΩ water into a 250 mL volumetric flask at room temperature, after which 0.69 mL of 18 M H_2SO_4 was added, followed by addition of 9.9 g (0.063 mol) of $KMnO_4$. The volumetric flask containing the mixture is then filled to 250 mL mark with 18 MΩ water, and then a magnetic stirring bar is introduced. The solution is then stirred for 10 minutes on a stirring plate at 300 rpm, at which state all solids are dissolved. The final solution is 0.25 M $KMnO_4$ in 0.05 M H_2SO_4. The same process is repeated to prepare the other two acidified $KMnO_4$ solutions in 0.01 M and 0.1 M H_2SO_4, which are properly adjusted for the volumes of H_2SO_4 needed. The second set of solutions is prepared in the manner described above except that the stirring is omitted. After the last step of filling the 250 mL volumetric flask containing the mixture to the mark, the solution is then shaken manually for 1 minute to further homogenize the mixture. Immediately after the solutions are prepared, with or without stirring, 10 mL of each solution is poured into 20 mL polyethylene scintillation vials, capped, and then aged stationary in the dark for 1–20 days. Identical experiment is repeated using glass scintillation vials to ensure that the result is not an artifact of using the polyethylene vials. For both cases, the aging is performed in the presence and absence of light. After the aging step, the vials are centrifuged at 4000 rpm for 10 minutes, decanted, and washed with 18 MΩ water 3 times to remove any unreacted permanganate. The solid samples are then air dried at room temperature for three days before characterization.

2.2. Characterization techniques

The manganese oxides were characterized by X-ray powder diffraction (XRD) using a PANalytical X'Pert PRO X-ray diffractometer with a CuK_α radiation (40 KV, 40 mA), and an X'Celerator solid state detector. The samples are prepared by suspending the oxide and the standard reference material (SRM) in ethanol to form a slurry. The oxide powders are prepared on a low-background silicon sample holder with the addition of an internal standard (NIST SRM 640c, $a = 5.43088$ Å). The patterns are recorded at room temperature with step-sizes of 0.008°, 2θ and 50 seconds. The phase constitutions are characterized using the International Center for Diffraction Data (ICDD) base for powder diffraction data. The crystal structure of the phase constitution is confirmed using Rietveld refinement (Topas 2.1 Bruker AXS) and the International Crystal Structure Data (ICSD) base.

The specific surface areas of the synthesized oxides are measured at 77 K using a Gemini 2370 (Micrometrics) surface and porosimetry instrument. The surface area is calculated by the Brunauer-Emmett-Teller (BET) [19] analysis of N_2 adsorption isotherm obtained after degassing and drying the sample at 200°C for 24 hours.

Scanning electron microscopy (SEM) images are obtained with the aid of a JEOL JSM-6700F field-emission SEM microscope. The samples for SEM analysis are prepared by placing 3 mg of the air dried solid manganese oxide on a black tape and then coating with carbon prior to SEM imaging.

Transmission electron microscopy (TEM) images were obtained with a Tecnai G^2 F30 S-Twin TEM instrument. The TEM operates at 300 KV using a field emission gun in Schottky mode as an electron source. The samples for TEM analysis are prepared by placing 3 mg of the air dried solid manganese oxide in 10 mL of 2-propanol, and sonication for 5 minutes for homogeneity. One drop of the slurry is deposited on a holey-carbon coated copper grid for analysis.

The thermogravimetric measurements (TGAs) are performed with a TA 2100 instrument at a heating rate of 20°C/min under nitrogen.

3. RESULTS

3.1. Formation of dendritic and spiral clusters of nanoscale

3.1.1. Mass of the solid MnO_2 formed during the aging process (stirring and no stirring)

Figure 1 shows mass of solid MnO_2 formed from the decomposition of a 0.25 M $KMnO_4$ solution in 0.1 M (solid lines), 0.05 M (dashed lines), and 0.01 M (dotted lines) H_2SO_4 prepared by the two methods, with and without stirring. It appears that the rate of solid MnO_2 formation and the yield increases with the concentration of the acid in all cases. It is to be noted that the mass yields are the same regardless of stirring. We hypothesize that the mechanism to produce black birnessite by the organic reductant may be similar to the one from stirring since both produce Mn^{2+} and then this species is oxidized by MnO_4^- to MnO_2.

3.1.2. X-ray powder diffraction

The solids formed without stirring appear brown in color, while those with stirring appear black. In either case there is $KMnO_4$ remnant, as evidenced by color in the supernatant. The solid phases formed by the different methods are characterized by XRD. Figure 2(a) shows the XRD patterns of nanosized semicrystalline black birnessite obtained with the stirring process along with the analysis of the data using the Rietveld refinement. The XRD pattern of brown colored birnessite formed without stirring is shown in Figure 2(b). These patterns show that the profile parameter of the diffraction peaks of black and brown birnessite is of the same phase. The diffraction peaks of the brown birnessite (see Figure 2(b)) seem better defined, indicating possibly a slight increase in crystallinity and/or larger birnessite particles than the black birnessite.

3.2. SEM studies

The morphology of birnessite obtained by the two methods is examined by SEM. Figure 3 shows the SEM images of black and brown birnessites with cotton ball-like and cloud-like particles, respectively, with diameters smaller than 1 μm. At higher magnification (see Figures 3(b) and 3(d)), the cotton-ball-like particles appear to link together to form larger particles with well-defined patterns, whereas the cloud-like particles appear as aggregates of individual smaller particles with no particular shape.

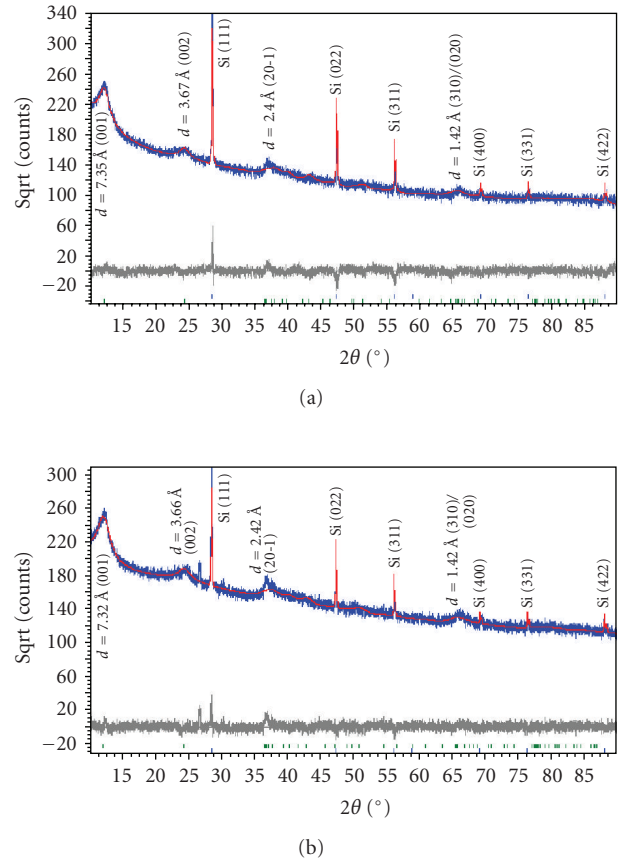

Figure 2: X-ray powder diffraction of the synthesized manganese oxides. (a) Black birnessite produced with stirring; (b) brown birnessite produced without stirring. The gray line in the bottom of both (a) and (b) is the pattern of the empty sample holder as a control.

3.3. TEM studies

The nanostructures of black and brown birnessites are studied by TEM. Figure 4 shows the TEM and HRTEM images of dendritic structure for the nanosized black birnessite produced with the stirring process. The sheets and dendritic architecture are represented in Figures 4(a) and 4(b). High-resolution electron microscopy (HRTEM) images in Figures 4(c) and 4(d) display the crystal structure of the fibrils [010] direction. Figure 4(c) shows the edge of a sheet and suggests that the sheets overlap. The high-resolution image in Figure 4(d) shows lattice fringes of the fibrils with a translation of 8-9 Å, which correspond well with the (001) lattice plane determined by XRD.

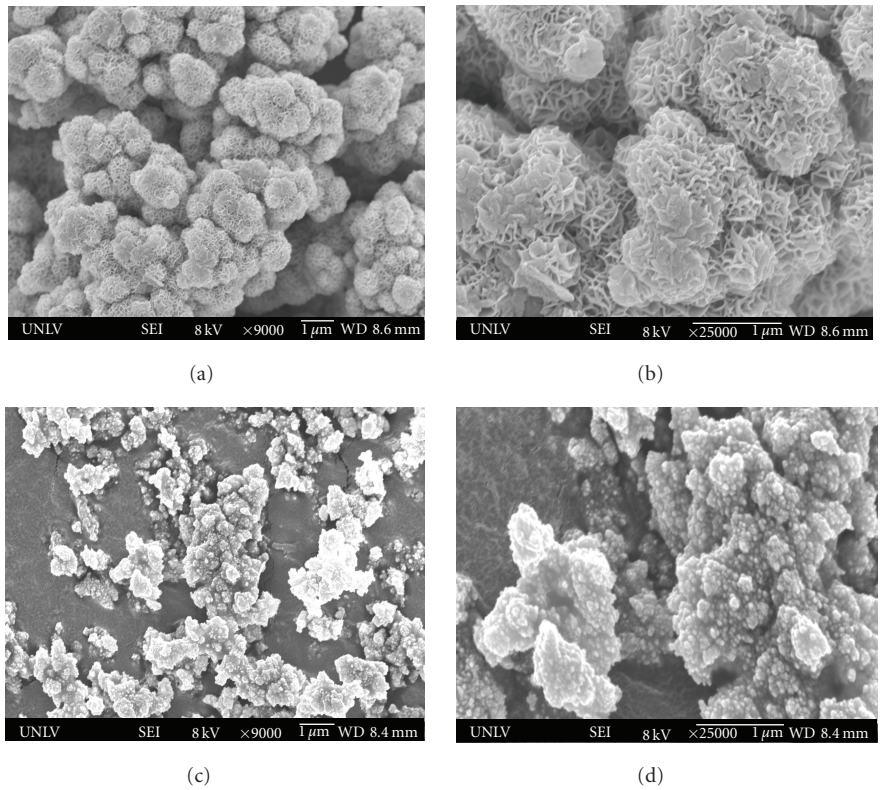

Figure 3: Scanning electron microscopy (SEM) images of (a) and (b) black and (c) and (d) brown birnessite nanomaterials.

Figure 5 shows the TEM and HRTEM images of the brown birnessite produced without the stirring process. The aggregated architecture is represented in Figures 5(a) and 5(b). Nanosized aggregates are observed with a discontinuous shape. The HRTEM images shown in Figures 5(c) and 5(d) show orientations of some of the fibrils in different direction. The dominant lattice fringes in the high-resolution images shown, however, indicate a repetition of the (001) lattice plane. Figure 5(d) also shows the spots of the individual atoms arranged in what appears to be a hexagonal structure. Figure 5(e) is an expansion of Figure 5(d) and is to be used to correlate the existing idealized structural model, obtained from EXAFS, shown in Figure 5(f).

It is interesting to note that when stirring is applied birnessite is formed not only on the bottom of the vial after centrifuging but also on the air-liquid interface in the form of a thin film. Figure 6 shows the TEM images of this film. The developing dendritic architecture is represented in Figures 6(a) and 6(b). The HRTEM images shown in Figures 6(c) and 6(d) suggest different orientation of some of the fibrils.

3.4. Thermal stability

TGA measurements are shown in Figure 7. The TGA profile for both black (see Figure 7(a)) and brown (Figure 7(b)) birnessite samples shows two similar weight losses. The first occurs with approximately 14% in the temperature range of 29–183°C, and the second occurs with approximately 4% in the range of 190–488°C. A slight mass gain is observed for the brown birnessite in the range of 480–544°C.

Table 1: Surface areas of the standard Kaolinite and synthesized birnessites.

Sample	Surface area (m^2/g)	Nanopore area (m^2/g)
Kaolinite-SRM lot no. 19672-18	15.3 (±1)	2.2 (±1)
Black birnessite	58.4 (±1)	4.3 (±1)
Brown birnessite	27.7 (±1)	4.1 (±1)

3.5. Surface area

The specific surface areas of birnessite nanoparticles are listed in Table 1. The values are of the same order as the ones obtained by other reductants such as HCl and $MnSO_4$ [14]. The aging time (not shown) appears to affect the surface area as well.

4. DISCUSSION

Permanganate ions in an acidic medium decompose according to the following reaction [21]:

$$4MnO_4^- + 12H^+ \longrightarrow 4Mn^{2+} + 5O_2 + 6H_2O. \quad (1)$$

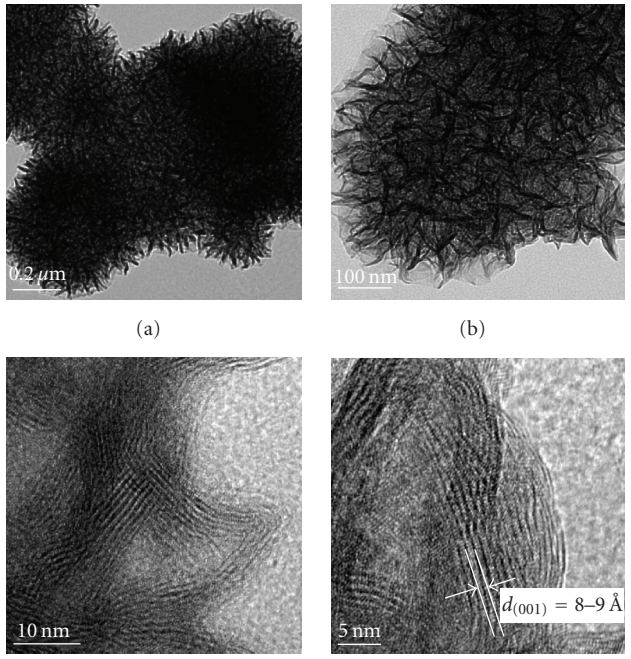

FIGURE 4: (a) and (b) TEM and (c) and (d) HRTEM images of the black birnessite nanomaterial produced with stirring.

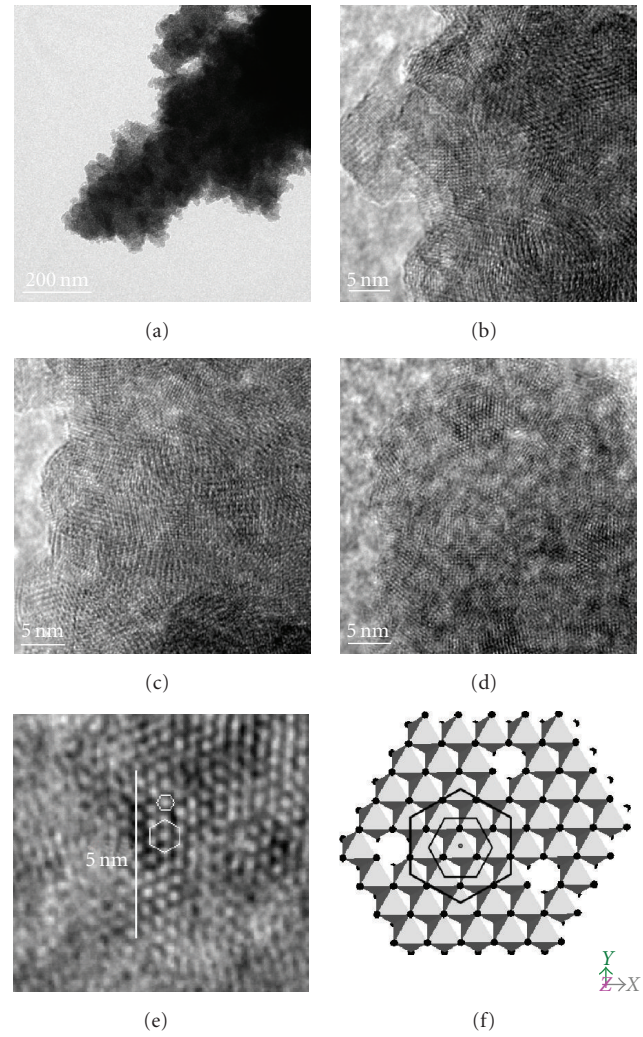

FIGURE 5: TEM and HRTEM images of the brown birnessite nanomaterial produced without stirring.

Subsequently, the Mn^{2+} produced reacts with permanganate ions to produce MnO_2:

$$2MnO_4^- + 3Mn^{2+} + 2H_2O \longrightarrow 5MnO_2 + 4H^+. \quad (2)$$

The overall reaction,

$$MnO_4^- + H^+ \longrightarrow MnO_2 + \frac{3}{4}O_2 + \frac{1}{2}H_2O, \quad (3)$$

shows that protons are reactants, thus explaining the increasing rate and yield with the acid concentration seen in Figure 1. The released oxygen may combine with Mn^{2+} from (1) to produce MnO_2 [22]. Permanganate reduction occurs via an $(MnO_3)_2$-SO_4 unstable intermediate [18, 22, 23], which slowly transforms to the manganese heptoxide Mn_2O_7 as

$$(MnO_3)_2\text{-}SO_{4(aq)} + H_2O_{(l)} \longrightarrow Mn_2O_{7(s)} + H_2SO_{4(aq)}. \quad (4)$$

The permanganate ion can be reduced to the lower valence MnO_2 species in acidic conditions via an intermediate Mn^{3+} [16] according to the redox reactions and oxidation potential diagrams [18]:

$$\begin{aligned}&\text{(Volts)}\quad 1.18 \quad -1.51 \quad -0.95 \quad -2.09 \quad -0.9\\ &Mn \longrightarrow Mn^{2+} \longrightarrow Mn^{3+} \longrightarrow MnO_2 \longrightarrow HMnO_4^- \longrightarrow MnO_4^-.\end{aligned} \quad (5)$$

The reduction potentials suggest that the manganic ion, Mn(III), produced by the reduction of permanganate ion by H_2SO_4 is unstable with respect to the decomposition reaction [22–24]:

$$2Mn(III) + 2H_2O \longrightarrow Mn(II) + MnO_2 + 4H^+. \quad (6)$$

The Mn(II) produced is then oxidized to Mn(IV) by permanganate (2). This can be a clue to the presence of traces of Mn(III) in the oxide. The contribution of SO_4^{2-} on the stabilization of Mn(III) in sulfuric acid media has been discussed previously [25]. In our method, the reaction between MnO_4^-, H_2SO_4, and H_2O does not seem to complete, as evidenced by the pink color of the solution at the end of the synthesis. The Mn(III) produced in this reaction is stable for months in acidic medium, such as in 4.5 M sulfuric acid. In our system, the sulfuric acid maximum concentration is 0.1 M, which makes both the Mn(III)-sulfate complex less stable [25] and the oxidation reaction of Mn(II) by permanganate slow [15]. This phenomenon presumably is responsible for the observed slow kinetics of MnO_2 production at low molar concentration of sulfuric acid (see Figure 1) and may explain why stirring has no effect on the total production of MnO_2.

XRD patterns of nanomaterials in Figure 2 show four major peaks whose positions and intensities seem to agree with those reported by Villalobos et al. [26] for acid

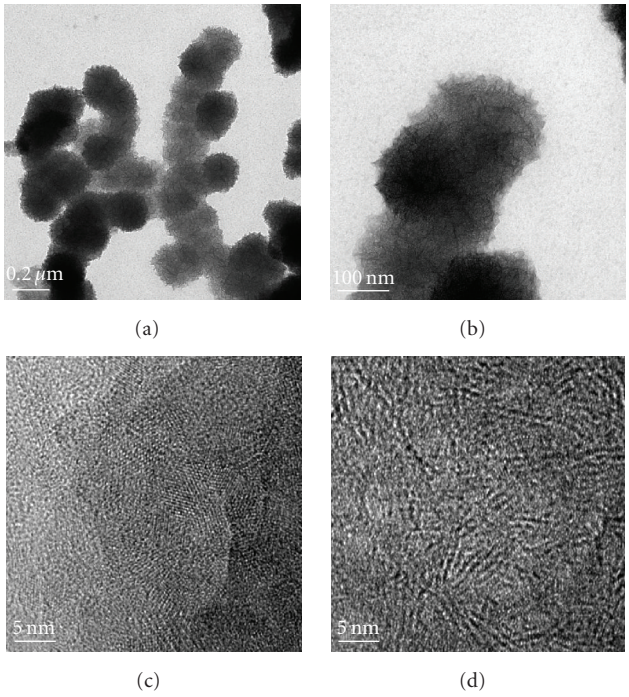

Figure 6: (a) and (b) TEM and (c) and (d) HRTEM images of the film formed on the air-liquid interface.

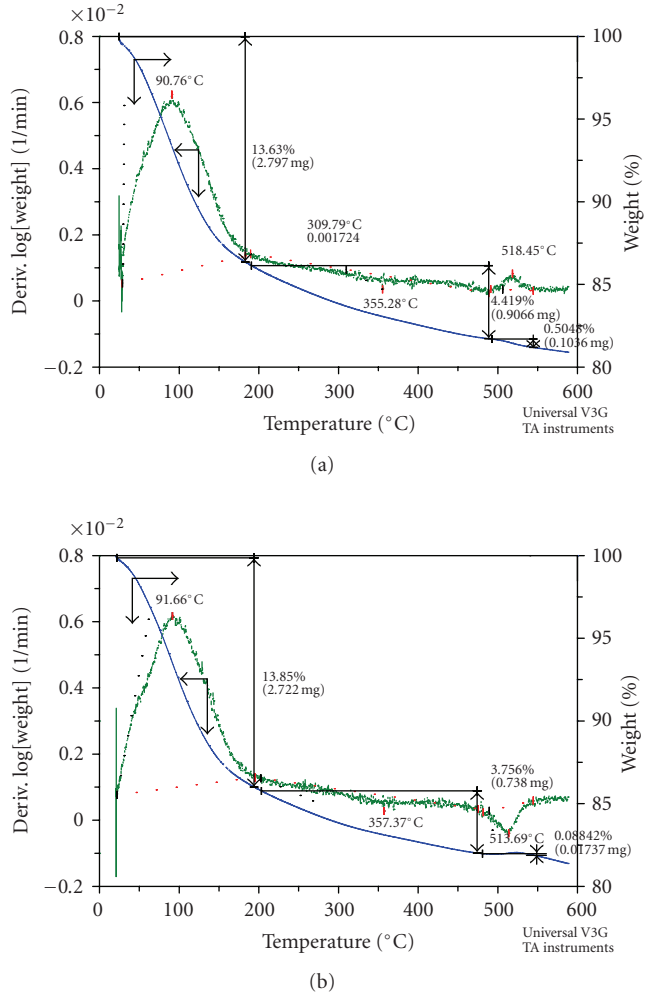

Figure 7: Thermogravimetric analysis (TGA) of the synthetic manganese oxides. (a) Black birnessite, (b) brown birnessite.

birnessite. The products with and without stirring are thus named as black and brown acid birnessites, respectively. To confirm the lamellar structure, a Rietveld refinement is done using the ICSD crystallographic data base. The two peaks at 7.35 and 3.67 Å correspond to 001 and 002 basal reflections, respectively, indicating an excellent agreement with other synthetic and natural birnessites. The broad humps at $2\theta = 50$–55° also look similar to those of acid birnessite reported by Villalobos et al. [26]. Additionally, the refined peak parameters indicate nanosize particles. One of the main differences between the birnessites obtained with and without stirring lies in the size of the particles, which is also evident from specific surface area values shown in Table 1. While both are nanosized, the black acid birnessite appears to form smaller crystallites, as evidenced by the slight less defined and lower-amplitude bands of its XRD pattern (see Figure 2), and by its larger specific surface area (see Table 1). We also note that without stirring, the solids formed tend to attach strongly onto the wall of both plastic and glass containers. There may be some catalysis on the surface of the containers, but it appears that colloids are formed first in solution and then adsorbed onto the container surface.

When stirring is applied initially during the synthetic process, the product obtained is composed mainly of plate-like fibrillar structures and black in color. The low-magnification SEM images of the manganese oxide synthesized show a raisin-like morphology with a diameter of less that 1 μm (see Figure 3). At high magnification, the raisin-like crystal morphology appears to consist of aggregates of plate-like crystals with diameters of ~0.5 μm linked tightly together. This plate-like crystal morphology seems identical to those reported for natural birnessites or their analogues obtained by different synthetic routes [5, 26]. This ubiquitous morphology indicates that in acidic conditions with stirring, MnO_2 has a structural shape preference attributed to that of the small sized of the building block (nanoscale embryo fibers). The product without the stirring process, on the other hand, seems highly aggregated and brown colored. It is intriguing to note that the 10 minutes initial stirring in an otherwise mostly stationary aging reaction of several days makes a considerable difference in the size and aggregation state of the particles obtained. SEM images of the manganese oxide synthesized without stirring show aggregates of cloud-like particles linked together with diameters of approximately 0.2 μm. The aggregates appear rough and discontinuous and do not show the plate-like crystal morphology seen in black birnessite. It is clear that one of the main reasons for the formation of birnessite with plate-like morphology in black birnessite is due to the brief mechanical agitation and not because of particular organic reductants used in the synthesis of this class of materials [2].

A closer look at the manganese oxide synthesized with initial stirring shows a dendritic and fibrous morphology (see Figure 4). The TEM images reveal that the length and width of the clusters are in the order of 300 nm and 200 nm, respectively. They also show that curled architectures are produced at the top of the dendrites. Formation of these clusters does not appear to depend on the aging time. Similar morphology has been obtained using the same synthesis (immediately after the 10 minutes stirring) but without aging time.

HRTEM studies show that most of the black birnessite nanofibers show (001) orientation; and the striations, evident along the length, indicate that they are arranged in different direction. In 5 nm length scale, the veins along the radial direction of the fiber are clearly seen, indicative of layered structure. This result supports the observation that the formation of the dendritic morphology may be due to the growth of a cluster of fibrous units along the *c*-axis, and that their small size produces a peak broadening in the XRD. Calculation of the *d*-spacing from the HRTEM images, using pixel resolution, gives $d = 8\text{-}9\,\text{Å}$, compared to $d = 7.3\,\text{Å}$ obtained by the XRD method. This difference is attributed to the poorly crystalline nature of the birnessite obtained. What is clear in black birnessite is that particles are made mainly of nanofibers characterized by homogeneous surfaces and uniform in size. We thus attribute its fibrillar dendritic morphology and formation to homogeneous nucleation. The production of the nanoscale fibers (embryos) seems to be a key step for the formation of dendritic morphology, and mechanical agitation affects both the morphology and the particle size. In this case, the nuclei may form spontaneously in the solution by stirring. The detailed mechanism for the formation of these interesting shapes at low pH is not presently known. However, we speculate that the formation of the sheets may be due to a structural control of crystal growth guided by osmotic pressure [27]. It is known that fibers or rods attract each other along their elongated sides forming clusters [28]. This phenomenon is evident in the TEM images. What is interesting is that the dendritic architectures observed in these inorganic nanomaterials are indeed similar to the structures observed using a variety of organic reductants [20], in biogenic manganese oxides [26] and in self-assembled organic systems [29]. It may explain why the surface area of black birnessite, which contains larger sheets, is higher ($58.4\,\text{m}^2\text{g}^{-1}$) than that of the brown birnessite, which contains much smaller sheets and cloud-like morphology. The black birnessite appears to be made up of small clusters of fibers linking together to form larger highly porous particles with high specific surface area.

The TEM image of the brown birnessite in Figure 5(a) shows cloud-like nanogranular morphology in the 200 nm range, similar to the aggregates produced from other materials, such as polymers [30]. It also suggests that the aggregates of brown birnessite are semicrystalline linked together to form larger clusters with no crystallographic orientation. HRTEM studies of this brown birnessite show particles composed of discontinuous nanofibers and individual atoms of Mn and O. The nanofibers are oriented in different directions, with their lattice fringes reflecting the (001) lattice plane. Individual atoms (spots) arranged in hexagonal form are also visible in the same sample at 5 nm resolution (see Figures 5(d)–5(e)). It is difficult to obtain a reasonable *d*-spacing value from the HRTEM images, using pixel resolution, probably due to the discontinuous nature and poor crystallinity of the material. However, due to this discontinuity and the fact that the spots of the individual atoms can be seen at 5 nm resolution, we are able to correlate for the first time an idealized structural model for birnessite, obtained by EXAFS spectroscopy, with our actual experimental observations (see Figures 5(d)–5(f)). The HRTEM image in Figure 5(e) clearly shows a hexagonal structural arrangement of the brown birnessite sheets (see large hexagon drawn in). Calculation of the equidistant magnitude between observed adjacent "spots" in this hexagonal arrangement yields a value of $4.8 \pm 0.2\,\text{Å}$, from pixel resolution. Comparing this value with the idealized structural hexagonal model proposed by Villalobos et al. [26] from modeling of EXAFS spectra, we find a close correlation with the Mn-Mn distance reported for second-shell neighbors around an Mn central atom of 4.99 Å (see Figure 5(f)), which would correspond also to second O-O neighbors in the sheet plane. Given this assignment, the first Mn-Mn (or O-O) shell, corresponding to a 2.88 Å distance [26], would be represented by the smaller hexagon depicted in Figures 5(e)–5(f). If this interpretation is correct, then the question remains as to why the hexagons observed are the ones from the second Mn (or O) shell, and not those from the first Mn (or O) shell. Further work needs to be done along these lines. It is clear from these images that no mechanical agitation produced a higher percentage of larger particles, which are composed of nanofibers with the individual atoms of Mn and O shown in hexagonal arrangement.

The film, produced after a few days of aging on the surface of the solution mixture for the stirred suspension, is characterized by XRD, and found to contain the same patterns as those in Figure 2(a). It is thus decided that the film material is black birnessite. The TEM and HRTEM images, shown in Figures 6(a)–6(d), also suggest that this film material is indeed the dendritic morphology observed for the material obtained from the bulk of the suspension (later stage of aging), shown in Figure 4. Furthermore, these images suggest the film material to be black birnessite with their fibrillar dendritic-like morphology in a developing stage. The HRTEM also shows transient embryos of nanofibers of about 5 nm in size that we believe are the basis for nucleation growth. The reason why these fibers are not destroyed by stirring may be due to the fact that they are less dense at this stage of development and accumulate in the surface of the mixture as a film, thus surviving the stirring and centrifuge processes. A possible mechanism for the formation of this structures and shapes would be as follows: (1) initially, nanofibers of MnO_2 form are forced to collide into each other; (2) upon collision, nucleation occurs in the surface of the particles; (3) once linked together, the particles grow into larger particles through aggregation. Although aggregation due to the van der Waals attraction is reversible, that due to the surface nucleation is not [30]. Energetically, this makes sense, and we conclude that the

acquired morphology observed in this work may be due to minimization of energy between the embryos and the substrate.

The TGA analysis shows that the birnessite nanoclusters prepared using the stirring and nonstirring methods have similar thermal profiles. The thermograms show two weight losses. The first loss of approximately 14% in the range of 29 to 183°C is due to loss of loosely bound water, indicating these samples are somehow hygroscopic. The second loss of approximately 4% in the temperature range of 190 to 488°C is attributed to chemically bound water and oxygen from the oxide [5]. There is in fact a small third weight loss of about 0.5% for the sample obtained with the stirring process (see Figure 7(a)) in the temperature range of 491–544°C, whereas a weight gain of about 0.09% is observed without the stirring in the temperature range of 480 to 544°C (see Figure 7(b)). It is attributed to migration of the Mn layer to the new vacant sites produced by the partial reduction of Mn^{4+} to Mn^{3+} and subsequent oxidation of Mn^{3+} by the freed oxygen in the local microenvironment [5]. The thermal stability of the samples appears unaffected by the wet-aging process.

5. CONDLUDING REMARKS

Black and brown birnessite nanoparticles are produced by the reaction of $KMnO_4$ in dilute aqueous H_2SO_4 medium with and without brief stirring, respectively, followed by a stationary aging at room temperature. Although the molecular structures of these two birnessites are similar, their morphologies are drastically different. The morphology of the brown birnessite, produced without the stirring process, correlates well with the theoretical hexagonal structural model of Villalobos et al. [26]. The morphology of the black birnessite, produced with the stirring process, appears similar to that prepared by other methods using organic reactants. In this study, black birnessites with dendritic morphology are produced for the first time via a reduction reaction of permanganate by dilute H_2SO_4 and without using any organic reactant, thus showing that the dendritic architecture is not induced by organic reactants. It is notable that a brief stirring in an early stage of the preparation can make a remarkable difference in the morphology of the product. The stirring process also produces black birnessite film on the air-liquid interface. A quantitative analysis associated with the stirring time and rate is a subject for future studies.

ACKNOWLEDGMENTS

This study is supported by the Special Research Grant of Yeungnam University. Authors thank Dr. Haesook Han for TGA thermograms of both black and brown birnessites and Nancy R. Birkner for helping with the BET method.

REFERENCES

[1] A. R. Armstrong and P. G. Bruce, "Synthesis of layered $LiMnO_2$ as an electrode for rechargeable lithium batteries," *Nature*, vol. 381, no. 6582, pp. 499–500, 1996.

[2] S. L. Brock, N. Duan, Z. R. Tian, O. Giraldo, H. Zhou, and S. L. Suib, "A review of porous manganese oxide materials," *Chemistry of Materials*, vol. 10, no. 10, pp. 2619–2628, 1998.

[3] Q. Feng, H. Kanoh, and K. Ooi, "Manganese oxide porous crystals," *Journal of Materials Chemistry*, vol. 9, no. 2, pp. 319–333, 1999.

[4] D. T. Vaniman, S. J. Chipera, D. L. Bish, M. C. Duff, and D. B. Hunter, "Crystal chemistry of clay-Mn oxide associations in soils, fractures, and matrix of the Bandelier Tuff, Pajarito Mesa, New Mexico," *Geochimica et Cosmochimica Acta*, vol. 66, no. 8, pp. 1349–1374, 2002.

[5] A.-C. Gaillot, B. Lanson, and V. A. Drits, "Structure of birnessite obtained from decomposition of permanganate under soft hydrothermal conditions. 1. Chemical and structural evolution as a function of temperature," *Chemistry of Materials*, vol. 17, no. 11, pp. 2959–2975, 2005.

[6] Z.-H. Liu, L. Kang, M. Zhao, and K. Ooi, "Preparation, ion-exchange, and electrochemical behavior of Cs-type manganese oxides with a novel hexagonal-like morphology," *Journal of Materials Research*, vol. 22, no. 9, pp. 2437–2447, 2007.

[7] A. Naidja, C. Liu, and P. M. Huang, "Formation of protein-birnessite complex: XRD, FTIR, and AFM analysis," *Journal of Colloid and Interface Science*, vol. 251, no. 1, pp. 46–56, 2002.

[8] R. A. Petrie, P. R. Grossl, and R. C. Sims, "Oxidation of pentachlorophenol in manganese oxide suspensions under controlled E_h and pH environments," *Environmental Science & Technology*, vol. 36, no. 17, pp. 3744–3748, 2002.

[9] J. Cai and S. L. Suib, "Preparation of layer structure birnessite by air oxidation: synthetic factors and framework dopant effects," *Inorganic Chemistry Communications*, vol. 4, no. 9, pp. 493–495, 2001.

[10] X. H. Feng, F. Liu, W. F. Tan, and X. W. Liu, "Synthesis of birnessite from the oxidation of Mn^{2+} by O_2 in alkali medium: effects of synthesis conditions," *Clays and Clay Minerals*, vol. 52, no. 2, pp. 240–250, 2004.

[11] D. C. Golden, C. C. Chen, and J. B. Dixon, "Synthesis of todorokite," *Science*, vol. 231, no. 4739, pp. 717–719, 1986.

[12] J. Luo and S. L. Suib, "Formation and transformation of mesoporous and layered manganese oxides in the presence of long-chain ammonium hydroxides," *Chemical Communications*, no. 11, pp. 1031–1032, 1997.

[13] J. Cai, J. Liu, and S. L. Suib, "Preparative parameters and framework dopant effects in the synthesis of layer-structure birnessite by air oxidation," *Chemistry of Materials*, vol. 14, no. 5, pp. 2071–2077, 2002.

[14] G. L. Clark and W. S. Coe, "Photochemical reduction with X-rays and effects of addition agents," *The Journal of Chemical Physics*, vol. 5, no. 2, pp. 97–105, 1937.

[15] M. A. Guyard, "Du dosage direct du manganese, de l'antimoine et de l'uranium par la methode des volumes et de quelques composes de ces metaux," *Bulletin de la Societe Chimique de France*, vol. 21, p. 89, 1864.

[16] M. Orbán and I. R. Epstein, "Minimal permanganate oscillator: the Guyard reaction in a CSTR," *Journal of the American Chemical Society*, vol. 111, no. 22, pp. 8543–8544, 1989.

[17] F. C. Tompkins, "A photoelectric turbidimeter for use in solution kinetics," *Transactions of the Faraday Society*, vol. 38, pp. 128–131, 1942.

[18] J. I. Morrow and S. Perlman, "A kinetic study of the permanganate-manganous ion reaction to form manganic ion in sulfuric acid media," *Inorganic Chemistry*, vol. 12, no. 10, pp. 2453–2455, 1973.

[19] S. Brunauer, P. H. Emmett, and E. Teller, "Adsorption of gases in multimolecular layers," *Journal of the American Chemical Society*, vol. 60, no. 2, pp. 309–319, 1938.

[20] R. M. McKenzie, "The synthesis of birnessite, cryptomelane, and some other oxides and hydroxides of manganese," *Mineralogical Magazine*, vol. 38, pp. 493–502, 1971.

[21] J. W. Ladbury and C. F. Cullis, "Kinetics and mechanism of oxidation by permanganate," *Chemical Reviews*, vol. 58, no. 2, pp. 403–438, 1958.

[22] L. Kótai, Á. Keszler, J. Pató, S. Holly, and K. K. Banerji, "The reaction of barium manganate with acids and their precursors," *Indian Journal of Chemistry*, vol. 38A, no. 9, pp. 966–968, 1999.

[23] W. M. Latimer and J. H. Hildebrand, *Reference Book of Inorganic Chemistry*, Macmillan, New York, NY, USA, 3rd edition, 1951.

[24] D. F. Shriver, P. Atkins, and C. H. Langford, *Inorganic Chemistry*, W. H. Freeman, New York, NY, USA, 2nd edition, 1994.

[25] M. A. Cheney, N. R. Birkner, L. Ma, et al., "Synthesis and characterization of inorganic double helices of cryptomelane nanomaterials," *Colloids and Surfaces A*, vol. 289, no. 1–3, pp. 185–192, 2006.

[26] M. Villalobos, B. Lanson, A. Manceau, B. Toner, and G. Sposito, "Structural model for the biogenic Mn oxide produced by *Pseudomonas putida*," *American Mineralogist*, vol. 91, no. 4, pp. 489–502, 2006.

[27] T. Terada, S. Yamabi, and H. Imai, "Formation process of sheets and helical forms consisting of strontium carbonate fibrous crystals with silicate," *Journal of Crystal Growth*, vol. 253, no. 1–4, pp. 435–444, 2003.

[28] S.-H. Yu, H. Cölfen, K. Tauer, and M. Antonietti, "Tectonic arrangement of $BaCO_3$ nanocrystals into helices induced by a racemic block copolymer," *Nature Materials*, vol. 4, no. 1, pp. 51–55, 2005.

[29] L. A. Estroff and A. D. Hamilton, "At the interface of organic and inorganic chemistry: bioinspired synthesis of composite materials," *Chemistry of Materials*, vol. 13, no. 10, pp. 3227–3235, 2001.

[30] D. Li and R. B. Kaner, "Shape and aggregation control of nanoparticles: not shaken, not stirred," *Journal of the American Chemical Society*, vol. 128, no. 3, pp. 968–975, 2006.

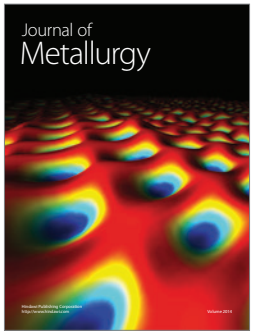

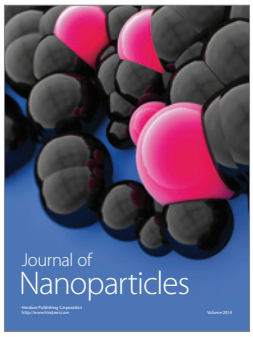

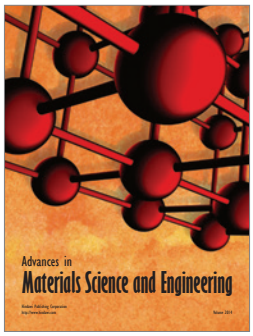

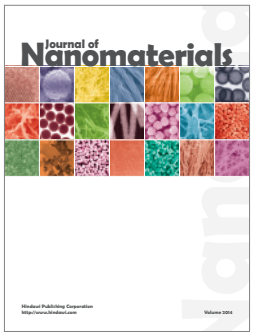

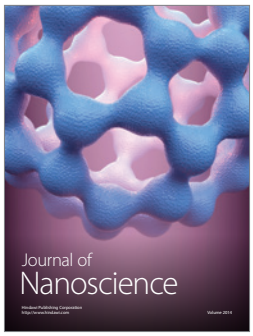

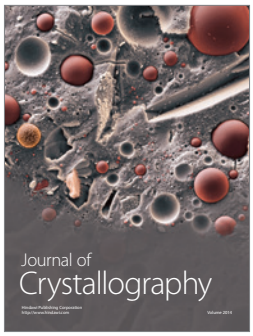

Hindawi

Submit your manuscripts at
http://www.hindawi.com